


Hydrodynamic Metamaterial Cloak for Drag-Free Flow

Juhyuk Park,¹ Jae Ryoung Youn,^{1,*} and Young Seok Song^{2,†}

¹*Research Institute of Advanced Materials (RIAM), Department of Materials Science and Engineering, Seoul National University, Seoul 08826, Republic of Korea*

²*Department of Fiber System Engineering, Dankook University, Gyeonggi Do 16890, Republic of Korea*

 (Received 8 March 2019; published 13 August 2019)

Metamaterials engineered based on transformation optics have facilitated inaccessible manipulation of various physical phenomena. However, such metamaterials have not been introduced for flowing viscous matter. Here we propose a hydrodynamic metamaterial cloak that can conceal an object in two-dimensional creeping flow by guiding viscous forces. Coordinate transformation of fluidic space is implemented to calculate a tensoric viscosity based on a form invariance of Navier-Stokes equations. The hydrodynamic cloak with the viscosity tensor is numerically simulated to verify a fictitious fluidic empty space created in it. The corresponding metamaterial microstructure is systemically designed and fabricated in a microfluidic device. The experimental results reveal that a solid object amid the flow can be hydrodynamically hidden without entailing a disturbance in flow fields and experiencing a drag.

DOI: [10.1103/PhysRevLett.123.074502](https://doi.org/10.1103/PhysRevLett.123.074502)

Fluidic drag is an inevitable phenomenon in aerodynamics and hydrodynamics as a frictional fluid force that acts on a solid object in the opposite direction to the fluid flow. In this sense, exclusion of such a drag force is a great challenge for scientific and engineering applications. Indeed, drag-free technology able to preclude frictional resistance to an object in flowing fluids can bring out a big impact on the fluid dynamics related industries such as vehicle body and building design [1].

Transformation optics has paved a breakthrough way for manipulating electromagnetic fields in an unprecedented manner [2,3]. It provides mathematical backgrounds for designing metamaterial cloaks that make an object inside it invisible [4]. This theory could be established based on a form invariance of Maxwell's equations using curvilinear coordinate transformations between different spaces. Furthermore, its concept has been applied to other areas, such as for thermodynamics [5,6], acoustics [7,8], dc electrics [9], solid mechanics [10,11], quantum mechanics [12], porous fluid flow [13,14], and time [15]. The metamaterials have been experimentally embodied by spatially varying the corresponding material parameters such as magnetic permeability using split-ring resonators [16], thermal conductivity using a composite made of copper and polydimethylsiloxane composite (PDMS) [5], and mechanical modulus using a porous microstructure [10]. Likewise, mapping of material parameters has been achieved by using sophisticatedly designed micro- or nanostructures.

The concept of fluid-dynamic cloaking was reported by leveraging coordinate transformation of Darcy's pressure equation and Brinkman-Stokes equation [13]. The authors reported that anisotropic mapping of permeability tensor

enables the cloaking of porous flow and their subsequent studies have theoretically proposed active hydrodynamic metamaterials [14,17]. However, as they mentioned, it is impossible to achieve the fluidic cloaking with passive metamaterials since negative permeability is required to generalize such cloaking.

In this Letter, we report a strategy of hydrodynamic cloaking that can manipulate viscous flow around an object by utilizing a metamaterial approach. Unlike the existing hydrodynamic cloak that exclusively aims to porous flow, we sought another strategy using a passive metamaterial microstructure. Viscosity of Navier-Stokes equations is a key property of flowing matter to characterize hydrodynamic behaviors, which is regarded as a resistance to flow. Hence, it can be hypothesized that viscous flow can be manipulated by spatially varying the fluidic resistance, and this can materialize a hydrodynamic metamaterial cloak to generate an artificial fictitious fluidic space in it.

A fundamental concept of the hydrodynamic cloak is schematically illustrated in Fig. 1, where expected pressure contours and flow patterns are demonstrated. Unlike the bare case without anything in the fluid [Fig. 1(a)], a cylindrical obstacle placed in the fluid is naturally subject to a resistant hydrodynamic force [Fig. 1(b)]. As a result, the pressure field developed around it is distorted, and then the surrounding fluid can be disrupted and splashed, conceptually indicating the drag generation on the surface. Herein, our strategy is to create a drag-free space and locate the obstacle in it [Fig. 1(c)]. For the cloaking, the space of the cylindrical region ($0 < r < b$) should be mathematically compressed into the annular region ($a < r' < b$). Then, the empty space ($0 < r' < a$) is created in the coordinate system and the obstacle located inside it becomes

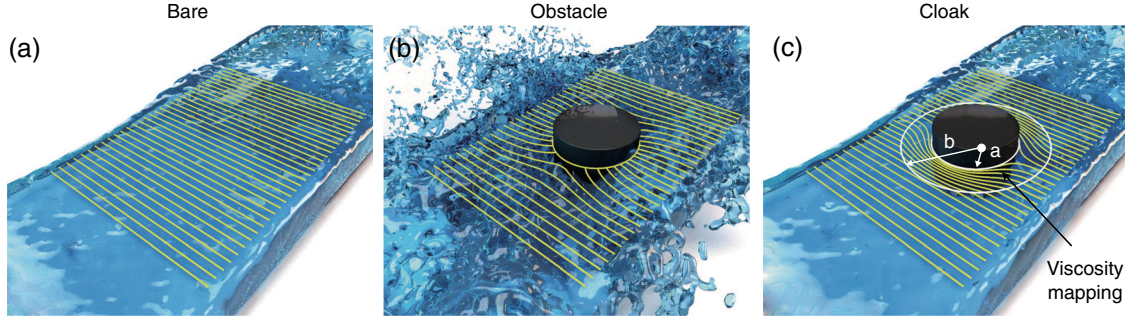


FIG. 1. Conceptual illustration of the hydrodynamic cloak. (a) Fluid flow in the bare space. (b) Fluid flow in the space with the obstacle. The obstacle amid the flow is subject to hydrodynamic force. (c) Fluid flow when the obstacle is encircled by the hydrodynamic cloak mapped with tensoric viscosity. The yellow lines indicate the pressure contour.

hydrodynamically transparent without undergoing any hydrodynamic forces [Fig. 1(c)]. The fluid flows as if there is no object within the flow field because the fluidic force cannot reach the cloaked space by detouring around there.

Indeed, transformation optics allows us to deduce that the mathematical form of Navier-Stokes equations is invariant under arbitrary coordinate transformations. Theoretical formulation of this transformation hydrodynamics was carried out to prove the form invariance of the Navier-Stokes equations [18]. Under assumptions of an incompressible Newtonian fluid at steady state with a low Reynolds number, the Navier-Stokes equations in the transformed space can be simplified as below [Eqs. (1) and (2)]:

$$\nabla' \cdot \tilde{\mathbf{u}}' = 0 \quad (1)$$

$$\nabla' \cdot \{ \tilde{\mu}' \cdot (\nabla' \tilde{\mathbf{u}}' + \nabla' \tilde{\mathbf{u}}'^T) \} = \nabla' p \quad (2)$$

where ∇' and $\tilde{\mathbf{u}}'$ are the nabla operator and the velocity field in the transformed space, respectively, p is the hydrostatic pressure and $\tilde{\mu}'$ is the second-order viscosity tensor defined as $\tilde{\mu}' = \det(\Lambda) \Lambda^{-1} \mu \Lambda^{-T}$, where μ is the viscosity of a fluid. Here, Λ indicates the Jacobian transformation matrix connecting the two different coordinate systems. Please note that the viscosity in Eq. (2) is no longer a scalar constant but a transformed tensor with an anisotropic spatial dependency.

For modeling the cloak, a linear geometric transformation shown in Fig. 2(a) is performed in the cylindrical coordinate system as follows: $r' = \{(b-a)/b\}r + a$, $\theta' = \theta$, $z' = z$ for $a < r' < b$, where a and b are the inner and outer radii of the cloak, respectively. The key concept is to compress a viscous force of the virtual space into a specific area of the physical space by using an anisotropic viscosity tensor. One point in the virtual space expands to the circular region of the physical space ($r' < a$), while the area outside the concentric circle ($r' > b$) remains intact [Fig. 2(a)]. The viscosity tensor, $\tilde{\mu}'$ for the ideal cloak is mathematically given by $\text{diag}[r'(r'-a), (r'-a)r']\mu$

(Fig. S1 [18]). The ideal cloak is not experimentally feasible due to extremely large variation in the tensoric viscosity components along both principal axes since the singular matrix problem occurs. In this respect, a reduced form of the viscosity tensor ($\tilde{\mu}''$) [Eq. (3)] is considered for mitigating experimental limitations [5,8,16,18].

$$\tilde{\mu}'' = \begin{bmatrix} \mu''_{rr} & \mu''_{r\theta} \\ \mu''_{\theta r} & \mu''_{\theta\theta} \end{bmatrix} = \begin{bmatrix} \left(\frac{b-a}{b}\right)^2 \left(\frac{r'}{r'-a}\right)^2 & 0 \\ 0 & \left(\frac{b-a}{b}\right)^2 \end{bmatrix} \mu \quad (3)$$

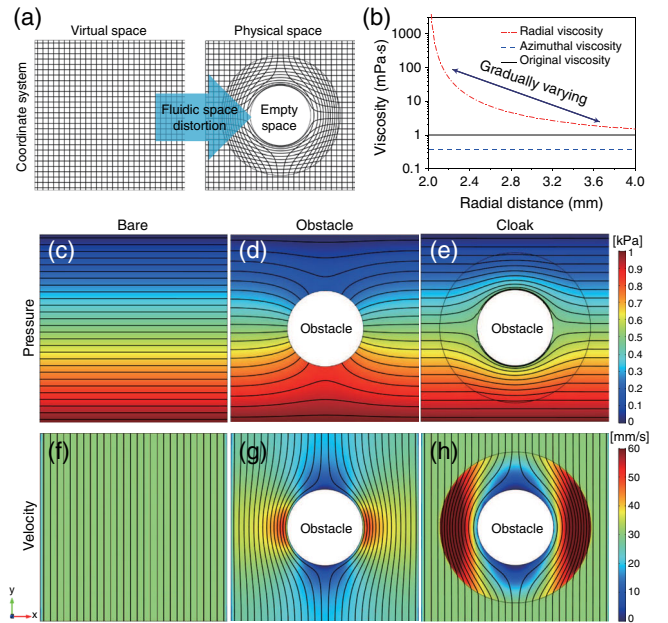


FIG. 2. Theoretical modeling of the hydrodynamic cloak. (a) Concept of coordinate transformation from virtual to physical spaces for cloaking a space. (b) Spatial profiles of the tensoric viscosity mapped on the cloaking shell in radial and azimuthal directions. Numerical simulation results of pressure (c)–(e) and velocity fields (f)–(h) simulated for the bare, obstacle, and cloak cases. The black lines in the images indicate the pressure contours (c)–(e) and streamlines (f)–(h), respectively.

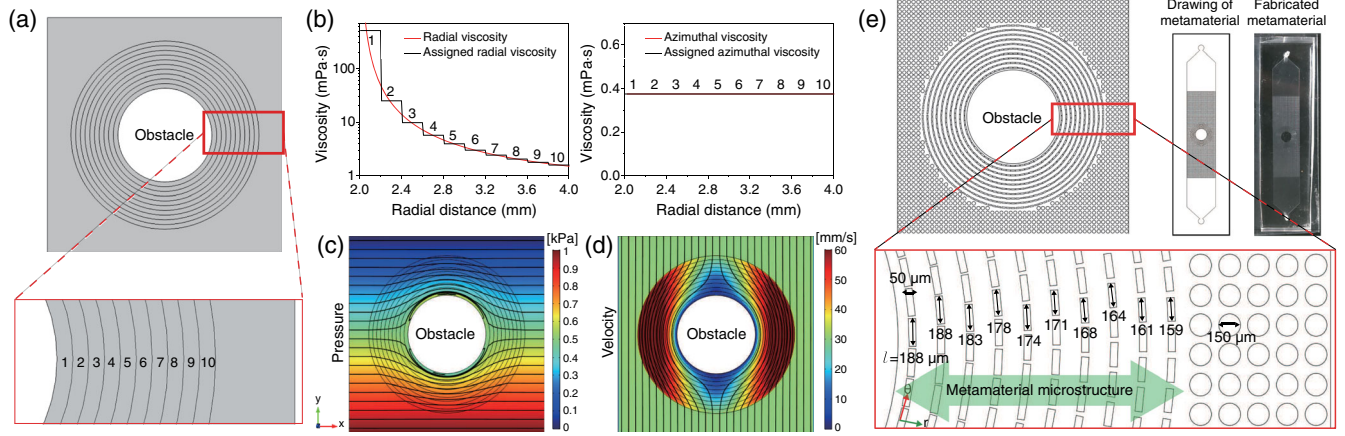


FIG. 3. Design and fabrication of the hydrodynamic metamaterial cloak. (a) Ten-layered structure of the multilayered cloak. (b) Discretized viscosity tensor in each layer along radial (left) and azimuthal (right) axes. The predicted pressure field (c) and velocity field (d) with the multilayered cloak. (e) Detailed configuration of the microstructured metamaterial.

The reduced viscosity tensor ($\tilde{\mu}''$) only varies in radial axis, but despite this modification it possesses a similar dispersion in the space as the ideal case from the point of cloaking success. The impedance mismatch at the outer boundary of the cloak is resolved by multiplying the viscosity tensor by a factor of 1.5 [16,19]. In this Letter, the viscosity tensor shown in Fig. 2(b) is used to simulate and design the hydrodynamic metamaterial cloak.

With the viscosity tensor, numerical simulation is conducted to demonstrate the hydrodynamic cloak using COMSOL MULTIPHYSICS, a commercial finite-element-based software. The dimensions of the simulated geometry are $1 \text{ cm} \times 1 \text{ cm} \times 50 \text{ }\mu\text{m}$. The diameters of the obstacle and the cloak are 4 and 8 mm, respectively. A pressure gradient of 1 kPa is applied from bottom to top. Figures 2(c) and 2(f) present the uniform pressure and velocity fields of the bare case with no perturbation in the domain. However, when an obstacle is placed in the fluid, dense pressure contours are generated on the obstacle surface. The resistant hydrodynamic forces are inevitably exerted on the obstacle surface and subsequently the pressure and velocity fields are disturbed severely [Figs. 2(d) and 2(g)].

Once the obstacle is encircled with the hydrodynamic cloak, the deviatoric stress of a flowing fluid cannot penetrate into the central region but rather detours around the obstacle [Figs. 2(e) and 2(h)]. This concealment removes the disturbance of velocity fields and creates straight streamlines outside the cloak, resulting in the flow field as the bare case. This implies that the object amid the flow can be hidden hydrodynamically since an external observer is unaware of the presence of the obstacle. The exclusion of viscous forces from the cloaked region leads to the significant increase in the velocity in the cloaking shell. This phenomenon occurs by virtue of the mapping of the tensoric viscosity, which directs the viscous forces toward the region with a lower viscosity component. For instance, the azimuthal viscosity in the cloaking shell is much lower than

the radial viscosity, and the flow is guided in the azimuthal direction accordingly. As a consequence, the cloaking region becomes a flow-free space with zero pressure gradient.

The drag force (F_d) and the drag coefficient (C_d) of the obstacle are calculated numerically. The drag force imposed on the obstacle surface is initially $115.2 \text{ }\mu\text{N}$ but decreases by about six times (i.e., $18.6 \text{ }\mu\text{N}$) after installing the cloak, and the drag coefficient is also reduced from 2802.0 to 440.8 as much as the drag force. While the calculated drag values do not become zero due to the mathematical iteration, the dramatic reduction in the drag is significant. Furthermore, if the obstacle is smaller than the size of the cloaked region, the resulting drag is negligible.

To implement the hydrodynamic cloak experimentally, first of all, a multilayered cloak [Fig. 3(a)] was designed based on the homogenized layer method [5,6,16], and it was subject to numerical analysis. The cloaking shell region ($a < r' < b$) is divided into ten annular layers, and the averaged viscosity components of the viscosity tensor are assigned to each layer [Fig. 3(b) and Table S1 [18]]. The viscosity distribution in the cloaking shell becomes discretized in a stepwise manner. The simulated pressure and velocity fields of the multilayered cloak [Figs. 3(c)–3(d)] verify the validity of design with a high degree of correspondence with the cloak with the continuous viscosity distribution [Figs. 1(e) and 1(h)] although a slight nonuniformity is observed at the interface of the layers.

Each layer on the multilayered cloak has different anisotropic viscosity tensors. Thus far, a variety of metamaterials have been strategically designed and fabricated into micro- or nanostructured devices that can control their own target physics such as electromagnetics [16,20], acoustics [8,21,22], elastomechanics [10,11], and thermodynamics [5,23]. By referring the report on microfabricated hydrodynamic metamaterials [24], we sought a way to achieve the viscous flow control by designing and situating anisotropic micropillars, as an effective viscosity unit cell,

on the metamaterial. It was expected that the micropillars can provoke different superficial flow velocities in each axis on the layers and this manipulation brings out such an effect of spatially changing anisotropic viscosity. Detailed specifications of the micropillars are designed based on numerical optimization [Fig. S2 and Table S2 [18]], the method is explained in [18]. At this step, the micropillar size should be smaller than the characteristic scale of momentum diffusivity of a fluid [5], water with a kinematic viscosity of $0.9 \text{ mm}^2/\text{s}$.

Prior to designing the metamaterial, all the viscosity components in Fig. 3(b) should be scaled up 3.5 times and the background area should be filled with microcylinders to avoid impedance mismatch at the interface between the metamaterial and background (Fig. S3 [18]) [5,10,11,21]. The length (l) of micropillars from the inside to outside of the cloaking layers varies from 188 to $159 \mu\text{m}$, while their thickness and height are fixed at $50 \mu\text{m}$ [Fig. 3(e)]. For anisotropic flow manipulation, the micropillars with a large aspect ratio are required. The micropillars are placed onto the cloaking shell layers at equal interval of $200 \mu\text{m}$, so the shell layers from inside to outside consist of 65, 72, 79, 85, 91, 97, 104, 110, 116, and 120 unit cells in order. Resultantly, the gap between micropillars on each layer is varying from $24 \mu\text{m}$ (layer 1) to $82 \mu\text{m}$ (layer 10) in azimuthal direction and keep constant distance of $150 \mu\text{m}$ in radial direction.

The designed microstructured metamaterial is numerically analyzed using COMSOL MULTIPHYSICS [Figs. 4(a)–4(i)]. The purpose of this simulation is to verify the possibility of hydrodynamic cloaking using not the viscosity tensor but the designed microstructure itself. The microstructured metamaterial can yield the same pressure and velocity fields with the cloaks with continuous and discretized viscosity distributions (Fig. S4 [18]). The isopressure contours are formed by deflecting the central cloaked area, indicating that there is a very small pressure gradient inside the cloaked region. The pressure and velocity contours outside the cloak are not disturbed by the existence of the cloaked obstacle. The drag force imposed on the obstacle is initially calculated as $110 \mu\text{N}$ but decreases by five times after installing the metamaterial, and the drag coefficient is also reduced fivefold. The reduction ratio of drag decreased slightly compared with the continuous medium and multilayer cases. These imperfections are presumably due to the error of the unit cell approximation.

The designed hydrodynamic metamaterial cloak is fabricated and experimentally validated using a microfluidic device. The microstructures of the considered cases are patterned onto silicon masters by employing photolithography and the microfluidic devices are manufactured using soft lithography. The streamlines of a flowing fluid in the microfluidic devices are visualized to verify the cloaking experimentally by using fluorescent microparticles. Detailed experimental methods are explained in the Supplemental Material [18].

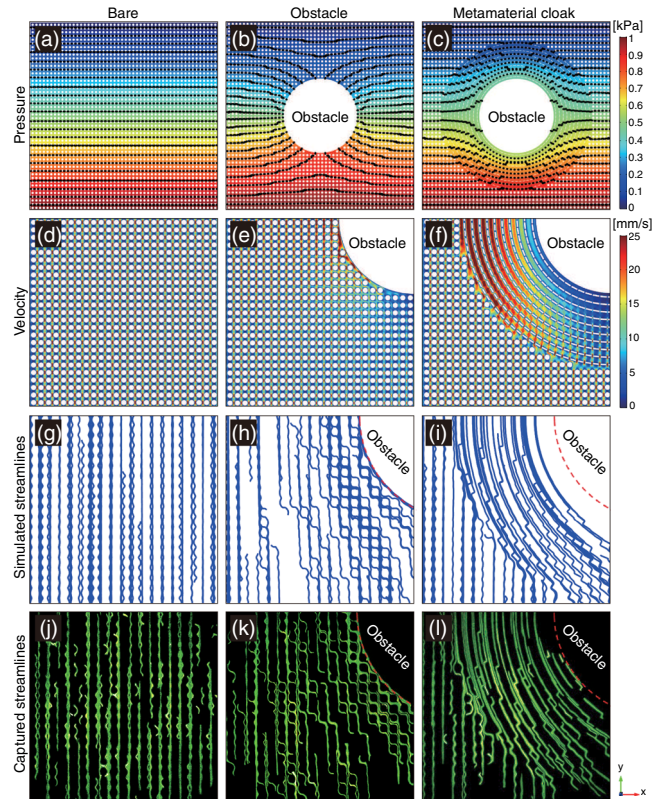


FIG. 4. Numerical and experimental validation of the hydrodynamic metamaterial cloak. Simulated pressure fields (a)–(c), velocity fields (d)–(f), and streamlines (g)–(i) for each microstructure. All the simulation results coincide with those from theoretical analyses shown in Fig. S4 [18]. Figures 4(j)–4(l) are the experimentally captured streamlines for each case. The red dashed lines indicate the obstacle surface.

Figures 4(j)–4(l) show the captured streamlines from the experiment, the same as those predicted numerically [Figs. 4(g)–4(i)]. The captured streamlines of the bare case [Fig. 4(j) and Movie S1] are found to have a parallel and uniform shape in all regions without being bent or interrupted, same as the simulation result. Unlike the bare case, the streamlines of the obstacle case are disturbed by hydrodynamic drag [Fig. 4(k) and Movie S2]. It is found that the green streamlines of flowing fluorescent particles are densely formed along the dashed red line which indicates the obstacle surface. This phenomenon means that the presence of the object can be perceived from a hydrodynamic point of view, and the overall flow rate of the microchannel is reduced by the drag generated when the fluid hits the obstacle surface.

When the obstacle is wrapped with the microstructured metamaterial cloak, it is shown that the obstacle can be hidden from viscous flow [Fig. 4(l) and Movie S3]. The streamlines outside the cloak remain in a parallel shape as if there is no obstacle amid the fluid. The flow path inside the metamaterial is very similar to the simulation results [Fig. 4(i)]. Also, unlike the obstacle case, the green

streamlines are hardly formed on the obstacle outline. It is the experimental evidence that there is little generation of drag on the obstacle surface. Furthermore, slowly moving particles in the vicinity of the obstacle indicate that the fluid flow is successfully bypassed around the obstacle with significantly low drag. Consequently, the experimental results demonstrate that the fluidic-cloaking is realized successfully in the microstructured metamaterial.

Despite this successful demonstration, there are some limitations of our cloaking metamaterial at this stage. Since the hydrodynamic metamaterial cloak is designed by a micropillar-mapping method, its practical applications are considerably limited. The biggest problem is that the viscosity components should be increased to several times the basic viscosity to make the fluid viscosity greater than 1. In the lab scale experiment, this issue was solved by mapping the microcylinders on the background area. To overcome this limitation, further advances in controlling viscosity are vitally required since the hydrodynamic metamaterial cloak itself cannot function alone in its present form. Also, the devised metamaterial cloak is designated to operate only for creeping flow with low Reynolds number. In the mathematical process, the Stokes flow condition was assumed not to consider the density tensor [18]. Therefore, the metamaterial cloak cannot bypass the fluid inertia force when confronting laminar flow. Furthermore, our metamaterial cannot handle turbulent flow. To resolve these problems, in-depth studies for laminar and turbulent flows are required by considering spatial mapping of anisotropic tensors of density and other turbulence-related terms.

In conclusion, we have demonstrated a new cloaking metamaterial to control viscous flow for drag-free technology. The anisotropic mapping of viscosity and its materialization enabled a solid amid flow to be cloaked in the flow field. We anticipate that this study will provide a new approaching way to fluidic dynamic problems with use of the hydrodynamic metamaterial.

This work was supported by GRRRC program of Gyeonggi Province (GRRRC Dankook2016-B03). In addition, this research was supported by Basic Science Research Program through the National Research Foundation of Korea (NRF) funded by the Ministry of Education (No. 2018R1D1A1B07049173) and by the Korea government (MSIT) (No. NRF-2018R1A5A1024127). The authors are grateful for the support.

*jaeryoun@snu.ac.kr

†ysong@dankook.ac.kr

- [1] R. Truesdell, A. Mammoli, P. Vorobieff, F. van Swol, and C. J. Brinker, Drag reduction on a patterned superhydrophobic surface, *Phys. Rev. Lett.* **97**, 044504 (2006).
 [2] U. Leonhardt, Optical conformal mapping, *Science* **312**, 1777 (2006).

- [3] J. B. Pendry, D. Schurig, and D. R. Smith, Controlling electromagnetic fields, *Science* **312**, 1780 (2006).
 [4] H. Chen, C. T. Chan, and P. Sheng, Transformation optics and metamaterials, *Nat. Mater.* **9**, 387 (2010).
 [5] R. Schittny, M. Kadic, S. Guenneau, and M. Wegener, Experiments on Transformation Thermodynamics: Molding the Flow of Heat, *Phys. Rev. Lett.* **110**, 195901 (2013).
 [6] S. Guenneau, C. Amra, and D. Veynante, Transformation thermodynamics: Cloaking and concentrating heat flux, *Opt. Express* **20**, 8207 (2012).
 [7] S. A. Cummer, B.-I. Popa, D. Schurig, D. R. Smith, J. Pendry, M. Rahm, and A. Starr, Scattering Theory Derivation of a 3d Acoustic Cloaking Shell, *Phys. Rev. Lett.* **100**, 024301 (2008).
 [8] S. Zhang, C. Xia, and N. Fang, Broadband Acoustic Cloak for Ultrasound Waves, *Phys. Rev. Lett.* **106**, 024301 (2011).
 [9] F. Yang, Z. L. Mei, T. Y. Jin, and T. J. Cui, Dc Electric Invisibility Cloak, *Phys. Rev. Lett.* **109**, 053902 (2012).
 [10] T. Bückmann, M. Thiel, M. Kadic, R. Schittny, and M. Wegener, An elasto-mechanical unfeelability cloak made of pentamode metamaterials, *Nat. Commun.* **5**, 4130 (2014).
 [11] T. Bückmann, M. Kadic, R. Schittny, and M. Wegener, Mechanical cloak design by direct lattice transformation, *Proc. Natl. Acad. Sci. U.S.A.* **112**, 4930 (2015).
 [12] S. Zhang, D. A. Genov, C. Sun, and X. Zhang, Cloaking of Matter Waves, *Phys. Rev. Lett.* **100**, 123002 (2008).
 [13] Y. A. Urzhumov and D. R. Smith, Fluid Flow Control with Transformation Media, *Phys. Rev. Lett.* **107**, 074501 (2011).
 [14] Y. A. Urzhumov and D. R. Smith, Flow stabilization with active hydrodynamic cloaks, *Phys. Rev. E* **86**, 056313 (2012).
 [15] R. W. Boyd and Z. Shi, Optical physics: How to hide in time, *Nature* **481**, 35 (2012).
 [16] D. Schurig, J. Mock, B. Justice, S. A. Cummer, J. B. Pendry, A. Starr, and D. Smith, Metamaterial electromagnetic cloak at microwave frequencies, *Science* **314**, 977 (2006).
 [17] D. Culver and Y. Urzhumov, Forced underwater laminar flows with active magnetohydrodynamic metamaterials, *Phys. Rev. E* **96**, 063107 (2017).
 [18] See Supplemental Material at <http://link.aps.org/supplemental/10.1103/PhysRevLett.123.074502> for mathematical demonstration of transformation hydrodynamics, detailed experimental and numerical methods, and additional data.
 [19] N. Stenger, M. Wilhelm, and M. Wegener, Experiments on Elastic Cloaking in Thin Plates, *Phys. Rev. Lett.* **108**, 014301 (2012).
 [20] J. Valentine, J. Li, T. Zentgraf, G. Bartal, and X. Zhang, An optical cloak made of dielectrics, *Nat. Mater.* **8**, 568 (2009).
 [21] M. Farhat, S. Guenneau, and S. Enoch, Ultrabroadband Elastic Cloaking in thin Plates, *Phys. Rev. Lett.* **103**, 024301 (2009).

- [22] H.F. Ma and T.J. Cui, Three-dimensional broadband ground-plane cloak made of metamaterials, *Nat. Commun.* **1**, 21 (2010).
- [23] S. Narayana and Y. Sato, Heat Flux Manipulation with Engineered Thermal Materials, *Phys. Rev. Lett.* **108**, 214303 (2012).
- [24] K. J. Morton, K. Loutnerback, D. W. Inglis, O. K. Tsui, J. C. Sturm, S. Y. Chou, and R. H. Austin, Hydrodynamic metamaterials: Microfabricated arrays to steer, refract, and focus streams of biomaterials, *Proc. Natl. Acad. Sci. U.S.A.* **105**, 7434 (2008).